Chinese Journal of Mechanical Engineering

ORIGINAL ARTICLE

Open Access

Active Fault Tolerant Nonsingular Terminal Sliding Mode Control for Electromechanical System Based on Support Vector Machine

Jian Hu[1*], Zhengyin Yang[1] and Jianyong Yao[1]

Abstract

Effective fault diagnosis and fault-tolerant control method for aeronautics electromechanical actuator is concerned in this paper. By borrowing the advantages of model-driven and data-driven methods, a fault tolerant nonsingular terminal sliding mode control method based on support vector machine (SVM) is proposed. A SVM is designed to estimate the fault by off-line learning from small sample data with solving convex quadratic programming method and is introduced into a high-gain observer, so as to improve the state estimation and fault detection accuracy when the fault occurs. The state estimation value of the observer is used for state reconfiguration. A novel nonsingular terminal sliding mode surface is designed, and Lyapunov theorem is used to derive a parameter adaptation law and a control law. It is guaranteed that the proposed controller can achieve asymptotical stability which is superior to many advanced fault-tolerant controllers. In addition, the parameter estimation also can help to diagnose the system faults because the faults can be reflected by the parameters variation. Extensive comparative simulation and experimental results illustrate the effectiveness and advancement of the proposed controller compared with several other main-stream controllers.

Keywords Aeronautics electromechanical actuator, Fault tolerant control, Support vector machine, State observer, Parametric uncertainty

1 Introduction

With the rapid development of electric technology, electromechanical actuator is more and more welcomed due to its relative cleanness, low noise, flexibility and convenient maintenance, compared to the electro-hydraulic servo actuation systems, which often have trouble with high noise, oil pollution and difficult maintenance and lead to a poor comfort for users. For example, both A320 aircraft and Boeing 787 have successfully substituted electric actuators for the traditional hydraulic actuator for some steering engines and conducted some test flights. NASA and others jointly developed an electric actuator for the X-33 and X-38 space shuttles [1, 2]. In addition, in the past, the controller of the aircraft actuator which was usually located in drivers' cab was far away from the actuator, which increased many additional equipment such as cables and connectors between the actuator and the flight controller, raised cost dramatically and at the same time reduced the reliability of the aircraft. Thus, the integrated design of actuators and controllers is more and more favored. However, by this way the controller will be moved from the original drivers' cab to the vicinity of the actuator, which deteriorates the controllers' working conditions dramatically and increases the probability of system fault greatly. Thus it is very important to make fault diagnosis and fault-tolerant control (FTC) of electromechanical actuators especially for safety-oriented aircraft engineering [3, 4].

*Correspondence:
Jian Hu
hujiannjust@163.com
[1] School of Mechanical Engineering, Nanjing University of Science and Technology, Nanjing 210094, China

There are mainly two kinds of fault tolerant control method including hardware redundancy and analytical redundancy method. Compared with the former, the latter can save the additional cost, space and complexity of hardware design, and thus the latter is more attractive although hardware redundancy is essential in many cases. Analytical redundancy method realizes fault tolerant control mainly by reconstructing some redundancy signals based on the mathematical model of the dynamic system.

With the progress of control theory and information technology, fault diagnosis based on model and analytical redundancy fault tolerant technology has made some breakthroughs in both linear and nonlinear systems [5–8]. However, in most of these studies the model uncertainties including parameter uncertainties and disturbance are combined with the possible fault for discussion, and thus the designed observer is not sensitive to the system fault. Yao et al. [9–11] carried out a lot of academic research, and pointed out that these uncertainties are the main reasons for the difficulty in design and implementation of model-based fault diagnosis methods. They creatively put forward a kind of nonlinear coordinate transformation based adaptive robust observer design method [9]. The parameter uncertainty and uncertain nonlinearity which exist widely in practical systems are fully considered. At the same time, the stability of the observer is ensured by the appropriate robust filtering, and the quantitative description of the parameter and state estimation error is given, which solves the problem that the observer design is easily disturbed by the modeling error. Based on the concept of parameter adaptive and robust filtering, Yao et al. designed the state reconstruction of the nonlinear system for the possible additive faults of the system. Then, the proposed parameter adaptive, state reconstruction and state observer were used to solve the common internal leakage and oil pollution faults of the electro-hydraulic servo system. The beneficial attempts of online detection, identification and controller regulation were made [12], and almost all system control performance could be recovered through targeted controller regulation. From the above analysis, it can be seen that Yao et al. mainly designs strategies of online monitoring system parameters and states with the nonlinear mathematical model of the system based on the analytical redundancy method, and then detects/identifies the possible faults of the system. This method balances the robustness and sensitivity of fault detection well, and it is of great value to ensure the safety of the system and carry out preventive maintenance in time. However, this method is still a model-based method, so it is necessary to establish an accurate mathematical model first which is not always practical in engineering. What's more, how to distinguish whether the system parameter aberration comes from malfunction or it is a normal drift with the change of working environment, and how to distinguish whether the system is faulty or subject to large external interference (such as aerodynamic load borne by aircraft steering gear) are major difficulties.

In recent years, data-driven methods based on neural networks have received more and more attention in the field of fault diagnosis and fault tolerant control [13–15]. Among these methods, SVM method is based on statistical learning theory, so it has an excellent ability to process data of nonlinear system. Especially, SVM algorithm has the optimization ability without knowing the specific model of the state, only according to a small amount of sample data while BP or some other neural networks need a large amount of sample data to learn and train themselves which degrade the learning efficiency. By training itself with the sample data, SVM can obtain a relationship between input and output, which is similar to a mapping law of the black box [16–18]. SVM classification and regression estimation methods show many advantages in solving small sample [19], pattern recognition [20], nonlinear model approximation [21], etc., which also provides new solutions for fault diagnosis of electromechanical servo systems with nonlinear characteristics.

In this paper, in order to have better performance of fault diagnosis and fault tolerant control, considering the fast response speed, high precision and finite time stability of terminal sliding mode controller [22, 23], this kind of controller is taken as a main controller. Then by borrowing the advantages of model-driven and data-driven methods, a fault tolerant nonsingular terminal sliding mode control method based on SVM is proposed. A SVM is designed to estimate the possible faults in the system by off-line learning from a small sample data with solving convex quadratic programming method. This estimation is used to compensate the possible fault with feedforward cancellation technique in the proposed observer and controller to improve the observer and tracking accuracy. The residual generated by the output of the observer and the real output of the system and the fault estimation value of SVM are used to comprehensively judge whether the system has faults, including sensor faults and actuator faults, so as to improve the accuracy of fault detection. The output of the observer is used to reconstruct the controller when something is wrong in aeronautics electromechanical system. Then Lyapunov theorem is used to design a nonsingular terminal sliding mode controller with a parameter adaptation law and to guaranteen an asymptotical stability of the proposed controller which is superior to many other fault-tolerant nonlinear controllers. In addition, the parameter estimation also

can be used to help diagnose the system faults since the faults can be reflected by the parameters variation.

The highlights of the proposed fault diagnosis and control method are as follows:

(1) A SVM capable of identifying faults by off-line learning from a small sample data is introduced into a high-gain observer, which helps improve the state estimation accuracy and reconfigure the controller more precisely.
(2) Considering that the frequency domain characteristics of the position signal can help judge whether the system malfunctions, Fourier transform method is used to extract the frequency mean of the position signal, which is taken as an input value of SVM to improve the fault detection performance**.**
(3) A novel nonsingular terminal sliding mode controller is designed, which can achieve asymptotical stability superior to many advanced fault-tolerant controllers.
(4) A parameter adaption law is also designed, which can help to diagnose the system faults because the faults can be reflected by the parameters variation.

This paper is organized as follows. Section 2 gives the problem formulation and system dynamic models. Section 3 presents the design process of fault detection method based on SVM. Section 4 shows the design procedure of nonsingular terminal sliding mode active fault tolerant controller. Section 5 carries out the comparative simulations and Section 6 carries out extensive experiments and analysis, and some conclusions can be found in Section 7.

2 Problem Description and Dynamic Model

Electromechanical actuator such as a steering engine driven by motors is usually composed of actuator , driver, mechanical transmission mechanism, inertia load, sensor (such as resolver, photoelectric encoder) and controller (as shown in Figure 1).

The actuator considered here is a permanent magnet motor with a commercial servo electrical driver. The motor works in a "current-controlled mode", that is to say, the control value of our controller u, which is output in the form of voltage, is a current command for the driver. The control value u is regarded as a value proportional to the output torque of the motor. Then we just denote the voltage-torque coefficient as k_{u}. Now our goal is to make the inertia load track any specified smooth motion trajectory $x_{1\mathrm{d}}$ as closely as possible. Considering all the above factors, the mathematical dynamic model of the electromechanical servo actuation system can be expressed as:

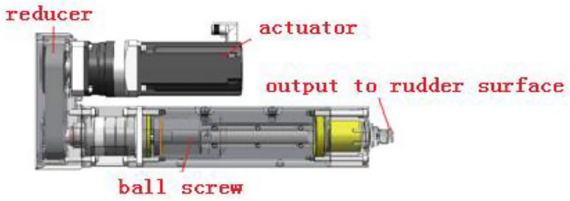

Figure 1 Block diagram of aeronautics electromechanical servo actuation system

$$m\ddot{y} = k_u u - B\dot{y} + d_0(y,\dot{y},t) + \eta(t) f_0(y,\dot{y},t), \tag{1}$$

where m is the equivalent inertia of the motor's rotor and load, y is the position of the inertia load, B is the equivalent viscous friction coefficient, $d_0(y,\dot{y},t)$ is the unmodeled dynamics, $f_0(y,\dot{y},t)$ represents the system fault characteristics related to time and state, and $\eta(t)$ is the time rule of fault occurrence.

$$\eta(t) = \begin{cases} 0, & \text{if } t < t_0, \\ 1 - e^{-\mu(t-t_0)}, & \text{if } t > t_0, \end{cases} \tag{2}$$

where μ is a constant, t_0 is the initial time of the fault occurrence.

Dividing two sides of Eq. (1) by m, we could obtain:

$$\ddot{y} = \theta_1 u - \theta_2 \dot{y} + d_n + f, \tag{3}$$

where $\theta_1 = k_u/m$, $\theta_2 = B/m$, $d_n = d_0/m$, and $f = \eta(t) f_0(y,\dot{y},t)/m$.

For the convenience of controller design, Eq. (3) can be rewritten in a state-space form as follows:

$$\begin{aligned} \dot{x}_1 &= x_2, \\ \dot{x}_2 &= \theta_1 u - \theta_2 x_2 + d_n(\boldsymbol{x},t) + f(\boldsymbol{x},t), \\ y &= x_1, \end{aligned} \tag{4}$$

where $\boldsymbol{x} = [x_1, x_2]^{\mathrm{T}} = [y, \dot{y}]^{\mathrm{T}}$ represents the state vector of the position and velocity, and set parameter $\boldsymbol{\theta} = [\theta_1, \theta_2]^{\mathrm{T}}$.

Considering the specific properties of parameters and disturbances of the electromechanical servo actuation system and to provide convenience for the design of controller, some assumptions should be made as follows.

Assumption 1 All the systematic parameters are invariant unknown variables or slowly time-varying unknown variables, that is to say, $\dot{\theta}_1 = \dot{\theta}_2 = 0$.

Assumption 2 All the systematic parameters are bounded and the upper/lower bounds are known. $\boldsymbol{\theta} \in \Omega_\theta = \{\boldsymbol{\theta} : 0 < \boldsymbol{\theta}_{\mathbf{min}} < \boldsymbol{\theta} < \boldsymbol{\theta}_{\mathbf{max}}\}$ where

$\boldsymbol{\theta}_{\max} = [\theta_{1\max}, \theta_{2\max}]^{\mathrm{T}}$ and $\boldsymbol{\theta}_{\min} = [\theta_{1\min}, \theta_{2\min}]^{\mathrm{T}}$ are the known upper/lower bounds of the parameters.

Assumption 3 $d_n(\boldsymbol{x}, t)$ is a time-varying unknown disturbance, but it is bounded, that is to say, $|d_n(\boldsymbol{x}, t)| \leq \delta_d$, where δ_d is a upper bound of the disturbance.

Assumption 4 System position tracking instruction signal $x_{1\mathrm{d}} \in C^2$ is bounded.

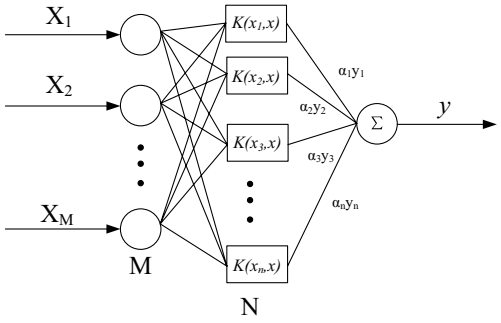

Figure 2 Structure diagram of support vector machines

3 SVM Based Fault Detection Method Design

Eq. (4) can be expressed in matrix form as follows:

$$\begin{aligned} \dot{\boldsymbol{x}} &= \boldsymbol{A}\boldsymbol{x} + \boldsymbol{B}u + \boldsymbol{D}(d_n + f), \\ y &= \boldsymbol{C}\boldsymbol{x}, \end{aligned} \tag{5}$$

where $\boldsymbol{A} = \begin{pmatrix} 0 & 1 \\ 0 & -\theta_2 \end{pmatrix}$, $\boldsymbol{B} = \begin{pmatrix} 0 & \theta_1 \end{pmatrix}^{\mathrm{T}}$, $\boldsymbol{D} = \begin{pmatrix} 0 & 1 \end{pmatrix}^{\mathrm{T}}$, $\boldsymbol{C} = (1 \ \ 0)$. According to the rank criterion of a time-invariant system, $rank[\boldsymbol{C}, \boldsymbol{C}\boldsymbol{A}]^{\mathrm{T}} = 2$ and thus system Eq. (5) is a second-order system satisfying the observability condition.

A classic high gain observer is as follows:

$$\begin{aligned} \dot{\hat{x}}_1 &= \hat{x}_2 + l_1(x_1 - \hat{x}_1), \\ \dot{\hat{x}}_2 &= -\theta_2\hat{x}_2 + \theta_1 u + l_2(x_1 - \hat{x}_1), \\ \hat{y} &= \hat{x}_1. \end{aligned} \tag{6}$$

It is obvious that when some faults occur in the system, the state observation accuracy of the high gain observer would decrease because it doesn't take the faults into consideration. To solve this problem, we introduce the faults estimation based on SVM into Eq. (6) and we could get the following nonlinear observer:

$$\begin{aligned} \dot{\hat{x}}_1 &= \hat{x}_2 + l_1(x_1 - \hat{x}_1), \\ \dot{\hat{x}}_2 &= -\theta_2\hat{x}_2 + \theta_1 u + \hat{f} + l_2(x_1 - \hat{x}_1), \\ \hat{y} &= \hat{x}_1. \end{aligned} \tag{7}$$

In Eq. (7), $\hat{x}_1$, $\hat{x}_2$ and $\hat{y}$ represent the position state observation value, velocity state observation value and system output observation value respectively, l_1 and l_2 represent the feedback gains of state observation error, and $\hat{f}$ represents the estimation of fault characteristics f by SVM. The structure of SVM is shown in Figure 2. By this way, the state observation accuracy of the observer could be improved when there is something wrong with the system which could help reconfigure the controller designed later more effectively.

Subtracting Eq. (7) from Eq. (4), we could get the error state equation as follows:

$$\begin{aligned} \dot{\tilde{x}}_1 &= -l_1\tilde{x}_1 + \tilde{x}_2, \\ \dot{\tilde{x}}_2 &= -l_2\tilde{x}_1 - \theta_2\tilde{x}_2 + d_n + f - \hat{f}, \\ \tilde{y} &= \tilde{x}_1, \end{aligned} \tag{8}$$

where $\tilde{x}_1 = x_1 - \hat{x}_1$, $\tilde{x}_2 = x_2 - \hat{x}_2$.

Based on the support vector machine regression method, given the sample data set $(\boldsymbol{x}_i, f_i)$ $(i = 1, 2, \ldots, n)$ where $\boldsymbol{x}_i$ represents the ith sample data of the state vector, a function in a higher dimensional eigenspace can be given to fit the sample set as follows:

$$\hat{f}(\boldsymbol{x}, t) = \boldsymbol{w}^{\mathrm{T}}\sigma(\boldsymbol{x}) + b, \tag{9}$$

where $\boldsymbol{w}$ is a weight vector, b is a offset quantity, and $\sigma(\cdot)$ is a RBF kernel function which could map the training data set from the input space to the high-dimensional feature space. Based on the theory of structural risk minimization, the fitting problem of Eq. (9) is transformed into the performance index of the optimization problem seeking the optimal solution:

$$\begin{aligned} &\min_{w,\xi^{(*)},b} J(\boldsymbol{w}) = \frac{1}{2}\boldsymbol{w}^{\mathrm{T}} \cdot \boldsymbol{w} + C\sum\left(\xi_i + \xi_i^*\right), \\ &\text{s.t.}, \ \ f_i - \boldsymbol{w}^{\mathrm{T}}\boldsymbol{\sigma}(\boldsymbol{x}) - b \leq \varepsilon + \xi_i, \\ &\qquad \boldsymbol{w}^{\mathrm{T}}\boldsymbol{\sigma}(\boldsymbol{x}) + b - f_i \leq \varepsilon + \xi_i^*, \\ &\qquad \xi_i, \xi_i^* \geq 0, \ \ (i = 1, 2, \ldots, n), \end{aligned} \tag{10}$$

where ξ_i, ξ_i^* are the relaxation variables. The significance lies in allowing certain misclassification of sample data under the condition that the sample data is not universal, that is, to ensure that the optimization problem has a solution without overlearning. The constant C represents the penalty index, which dominates the penalty degree of the misclassified sample. An insensitive loss function ε is selected according to the actual situation in the following form:

$$\left|f-\hat{f}\right|=\begin{cases}0, & \left|f-\hat{f}\right|\le\varepsilon,\\ \left|f-\hat{f}\right|-\varepsilon, & \left|f-\hat{f}\right|>\varepsilon.\end{cases} \tag{11}$$

The introduction of ε-insensitive loss function can help system be robust to system failures to a certain extent, so that the prediction error can be within a certain range. When the system has no additive failure, the SVM output $\hat{f}$ is 0.

Literature has theoretically proved that kernel-based SVM can approximate a continuous function arbitrarily. Due to the model uncertainty and interference inherent in the system, the following inequalities hold:

$$\left|f(\boldsymbol{x},t)-\hat{f}(\boldsymbol{x},t)\right|\le F,\quad F>0, \tag{12}$$

where F is a constant.

Transform observer Eq. (7) into matrix expression form as follows:

$$\begin{aligned}\dot{\hat{\boldsymbol{x}}}&=\boldsymbol{A}\hat{x}+\boldsymbol{B}u+\boldsymbol{L}(y-\hat{y})+\boldsymbol{D}\hat{f}(\hat{\boldsymbol{x}},t),\\ \hat{y}&=\boldsymbol{C}\hat{\boldsymbol{x}},\end{aligned} \tag{13}$$

where $\boldsymbol{L}=[l_1,l_2]^{\mathrm{T}}$, and according to Eq. (7) and Eq. (12), the dynamic equation of system error can be obtained as follows:

$$\begin{aligned}\dot{\boldsymbol{e}}_x&=(\boldsymbol{A}-\boldsymbol{LC})\boldsymbol{e}_x+\boldsymbol{D}\left(d_n+f-\hat{f}\right),\\ \dot{e}_y&=\boldsymbol{C}\boldsymbol{e}_x,\end{aligned} \tag{14}$$

where state observation error $\boldsymbol{e}_x=\boldsymbol{x}-\hat{\boldsymbol{x}}$ and system output error $e_y=y-\hat{y}$.

By combining Eqs. (7) and (13), we can get the following relations:

$$\boldsymbol{A}_o=\boldsymbol{A}-\boldsymbol{LC}=\begin{pmatrix}-l_1 & 1\\ -l_2 & -\theta_2\end{pmatrix}. \tag{15}$$

Select the gain matrix $\boldsymbol{A}_o$ of the observer to be a Hurwitz stable matrix that satisfies the Riccati equation as follows:

$$\boldsymbol{A}_o^{\mathrm{T}}\boldsymbol{P}+\boldsymbol{P}\boldsymbol{A}_o=-\boldsymbol{Q},\quad \boldsymbol{P}=\boldsymbol{P}^{\mathrm{T}}>0,\quad \boldsymbol{Q}>0, \tag{16}$$

where $\boldsymbol{P}$, $\boldsymbol{Q}$ are the positive definite matrix and $\boldsymbol{P}=\boldsymbol{P}^{\mathrm{T}}>0$.

The selection of input signal of SVM also has an important influence on its approximation performance to the fault. Considering the frequency domain characteristics of the position signal, such as frequency mean, center frequency, can help judge whether the system malfunctions, in this paper, Fourier transform method is used to extract the frequency mean of the position signal, which is taken as an input value of SVM, together with position and speed signals as the input vector, so as to improve the fault identification performance. Thus, the input vector of SVM is chosen as $\boldsymbol{x}=[\overline{x}_{1f},x_1,x_2]^{\mathrm{T}}$, where $\overline{x}_{1f}$ is the frequency mean of the position signal.

Theorem 1 The observation error of the observer Eq. (13) with SVM based fault estimation Eq. (9) is bounded.

Proof See the Appendix.

Remark 1 The fault in the system can be detected according to $\hat{f}(\overline{x}_{1f},x_1,x_2)$ and whether the system fails can be judged by whether the detected value $\hat{f}(\overline{x}_{1f},x_1,x_2)$ exceeds a certain threshold. However, since the fault is taken into account in Eq. (7), the states observation residual $e_x(t)=\sqrt{(x_1-\hat{x}_1)^2+(x_2-\hat{x}_2)^2}$ would be small and we could not judge whether there is a fault in the system according to $e_x(t)$ now. We only could use the residual of Eq. (6) to help implement system fault identification, which can be combined with $\hat{f}(\overline{x}_{1f},x_1,x_2)$ detection results, so as to improve the accuracy of fault detection.

In this method, fault estimation uses data-driven method and support vector machine is used to detect faults through feature extraction, fault classification and recognition. Therefore, it is not affected by system model and also can get rid of the influence of system disturbance. In addition, it is combined with the model driven method to further improve the accuracy of fault detection and avoid false alarm. In this method, the selection of threshold is particularly critical and it can be chosen appropriately in advance according to engineering experience.

Whether a fault-tolerant control is implemented depends on the results of fault detection. If the fault is very small, there is no need for a fault-tolerant control to implement because the robust item in a controller can conquer it. If the fault is large and lies in a certain threshold range, fault-tolerant control can be carried out to compensate the fault and diminish its influence as possible as it can. However, if the fault is very large and even exceeds a certain threshold, a serious fault is indicated and at this time fault-tolerant control is incapable of action, so other measures such as preventive maintenance need to be taken.

Remark 2 The selection of training samples is particularly crucial for approximation performance of SVM. We select a large number of working conditions, including normal working conditions, actuator failure working conditions, sensor failure working conditions, and composite failure working conditions, and collect system state information under various working conditions as input, with known faults as output, so that the samples cover various working conditions as much as possible.

By this way, SVM can obtain an excellent approximation performance.

4 Active Fault Tolerant Non-Singular Terminal Sliding Mode Controller Design

Step 1: Sliding mode surface design

Define tracking error as follows:

$$\begin{aligned} e_0 &= x_1 - x_{1\mathrm{d}}, \\ e_1 &= \dot{e}_0, \\ e_2 &= \dot{e}_1 = \ddot{e}_0, \end{aligned} \tag{17}$$

$x_{1\mathrm{d}}$ is the command signal, e_0, e_1 and e_2 are the tracking errors of position, velocity and acceleration respectively.

A sliding mode surface is designed as follows:

$$\sigma_1 = e_0 + \alpha \mathrm{sgn}^{\lambda_1}(e_0) + \beta \mathrm{sgn}^{\lambda_2}(e_1), \tag{18}$$

where α>0, β>0, λ_1>1, λ_2>1, and

$$\mathrm{sgn}^{\lambda}(e) = |e|^{\lambda}\mathrm{sgn}(e) = \begin{cases} e^{\lambda}, & e > 0, \\ 0, & e = 0, \\ -(-e)^{\lambda}, & e < 0, \end{cases} \tag{19}$$

Differentiating the sign function term $\mathrm{sgn}^{\lambda}(\cdot)$, we could get:

$$(\mathrm{sgn}^{\lambda}(e))' = \begin{cases} \lambda |e|^{\lambda-1}\dot{e}, & e \neq 0, \\ 0, & e = 0. \end{cases} \tag{20}$$

The design idea of Eq. (18) is illustrated as follows: when the initial system position tracking error is large, the function of $\alpha \mathrm{sgn}^{\lambda_1}(e_0)$ is stronger than that of $\beta \mathrm{sgn}^{\lambda_2}(e_1)$. When the position tracking error slowly converges to zero, $\beta \mathrm{sgn}^{\lambda_2}(e_1)$ dominates the convergence of speed tracking error.

Meanwhile, in order to realize continuous nonsingular terminal sliding mode control, a sliding mode surface is redesigned combining with integral sliding mode as follows:

$$\begin{aligned} \sigma_2 &= \sigma_1 - e_0 + s \\ &= \alpha \mathrm{sgn}^{\lambda_1}(e_0) + \beta \mathrm{sgn}^{\lambda_2}(e_1) + ce_0 + e_1 + k_i \int_0^t e_0 \mathrm{d}\tau, \end{aligned} \tag{21}$$

where

$$s = ce_0 + e_1 + k_i \int_0^t e_0 \mathrm{d}\tau, \tag{22}$$

and c, k_i are constants.

The sign function of sliding mode control makes the controller discontinuous in design. Therefore, by further differentiating the sign function term $\mathrm{sgn}^{\lambda}(\cdot)$ defined in the sliding mode surface switching function Eq. (21), namely differentiating Eq. (21), the control term $\mathrm{sgn}^{\lambda}(\cdot)$ is continuous and non-singular in the case of time continuity according to Eqs. (19) and (20). Therefore, the derivative of Eq. (21) is obtained as follows:

$$\begin{aligned} \dot{\sigma}_2 &= \dot{\sigma}_1 - \dot{e}_0 + \dot{s} \\ &= \alpha\lambda_1 |e_0|^{\lambda_1 - 1} \cdot e_1 + \beta\lambda_2 |e_1|^{\lambda_2 - 1} \cdot \dot{e}_1 + \dot{s} \\ &= \left(c + \alpha\lambda_1 |e_0|^{\lambda_1 - 1}\right) \cdot e_1 + \left(1 + \beta\lambda_2 |e_1|^{\lambda_2 - 1}\right) \\ &\quad \cdot \left(\theta_1 u - \theta_2 x_2 + d_n + f - \ddot{x}_{1d}\right) + k_i e_0. \end{aligned} \tag{23}$$

Denote ρ_1 and ρ_2 as follows:

$$\rho_1 = \alpha\lambda_1 |e_0|^{\lambda_1 - 1}, \alpha > 1, \lambda_1 > 1, \tag{24}$$

$$\rho_2 = \beta\lambda_2 |e_1|^{\lambda_2 - 1}, \beta > 1, \lambda_2 > 1. \tag{25}$$

Obviously, Eqs. (24) and (25) are continuous. Therefore, Eq. (23) can be expressed as:

$$\begin{aligned} \dot{\sigma}_2 &= (c + \rho_1) \cdot e_1 + k_i e_0 \\ &\quad + (1 + \rho_2) \cdot \left(\theta_1 u - \theta_2 x_2 + d_n + f - \ddot{x}_{1d}\right). \end{aligned} \tag{26}$$

Step 2: Control law design

Therefore, a parameter-adaption based non-singular terminal sliding mode controller (PANTSMC) can be designed:

$$\begin{aligned} u &= \frac{1}{(1 + \rho_2)\hat{\theta}_1}(u_a + u_s), \\ u_a &= -(1 + \rho_2) \cdot \left(-\hat{\theta}_2 \hat{x}_2 + \hat{f} - \ddot{x}_{1d}\right) - [(c + \rho_1) \cdot e_1 + k_i e_0], \\ u_s &= u_{s1} + u_{s2}, \qquad u_{s1} = -k_1 \sigma_2. \end{aligned} \tag{27}$$

In Eq. (27), u_a represents a model feedforward compensation term, and is carried out by real-time updating estimation of parameter and state estimation. u_{s1} represents a linear feedback term, and k_1>0 is a tunable parameter of the linear feedback term. u_{s2} represents a nonlinear robust feedback term, which has a strong robustness effect.

Step 3: Parameter adaptive law design

An adaptive law is designed for the system parameters $\hat{\boldsymbol{\theta}}$, which is taken from the following adaptive function:

$$\boldsymbol{\tau} = \boldsymbol{\varphi}\sigma_2, \tag{28}$$

where $\boldsymbol{\varphi} = (u \quad -x_2)^{\mathrm{T}}$.

The adaptive law of system parameters is designed as follows:

$$\dot{\hat{\boldsymbol{\theta}}} = (1 + \rho_2) \cdot \mathrm{Proj}_{\hat{\theta}}(\boldsymbol{\Gamma}\boldsymbol{\tau}) - k_\theta \hat{\boldsymbol{\theta}}, \tag{29}$$

where $k_\theta > 0$, $\boldsymbol{\Gamma}$ represents a positive definite diagonal adaptive rate matrix.

Define the discontinuous mapping function as follows:

$$\mathrm{Proj}_{\hat{\theta}_i}(\tau_i) = \begin{cases} 0, & \text{if } \hat{\theta}_i = \theta_{i\max} \text{ and } \tau_i > 0, \\ 0, & \text{if } \hat{\theta}_i = \theta_{i\min} \text{ and } \tau_i < 0, \\ \tau_i, & \text{otherwise.} \end{cases} \tag{30}$$

Step 4: Disturbance upper bound adaptive law design

In general, it is difficult to know δ_d in Assumption 3 according to objective conditions and thus an adaptive law of the disturbance upper bound is designed here:

$$\dot{\hat{\delta}}_d = (1+\rho_2)\gamma|\sigma_2| - k_\delta \hat{\delta}_d, \tag{31}$$

where $\hat{\delta}_d$ is the estimation of δ_d, and $k_\delta > 0$.

As the denominator $(1+\rho_2)\hat{\theta}_1$ is always greater than 0, controller Eq. (27) is completely non-singular. Substituting the controller Eq. (27) into Eq. (26), we can get:

$$\begin{aligned} \dot{\sigma}_2 =& -k_1\sigma_2 + u_{s2} + (1+\rho_2)\left(\tilde{\theta}_1 u - \tilde{\theta}_2 x_2 + \hat{\theta}_2\tilde{x}_2 + d_n + \tilde{f}\right) \\ =& -k_1\sigma_2 + u_{s2} + (1+\rho_2)\left(-\tilde{\boldsymbol{\theta}}^{\mathrm{T}}\boldsymbol{\varphi} + \hat{\theta}_2\tilde{x}_2 + d_n + \tilde{f}\right), \end{aligned} \tag{32}$$

where $\tilde{f} = f - \hat{f}$.

Step 5: Robust term design

In general, there always exist some errors between the real values and the estimation values of system parameters θ and it is the same for δ_d and $\hat{\delta}_d$. Thus it is necessary to construct a nonlinear robust feedback item u_{s2} to overcome the influence of system parameter estimation error $\tilde{\boldsymbol{\theta}}$, disturbance upper bound estimation error $\tilde{\delta}_d$ and SVM observation error $\tilde{f}$, in order to improve the stability and accuracy of the system.

The designed nonlinear robust term $u_{s2} = u_{s21} + u_{s22}$ should satisfy:

$$\sigma_2 u_{s21} \le 0, \sigma_2 u_{s22} \le 0, \tag{33}$$

$$\sigma_2\left[u_{s21} + (1+\rho_2)\left(\hat{\theta}_2\tilde{x}_2 + \tilde{f}\right)\right] \le \varepsilon_{\sigma 1}, \tag{34}$$

$$\sigma_2\left[u_{s22} + (1+\rho_2)\left(d_n + \tilde{\delta}_d \mathrm{sgn}(\sigma_2)\right)\right] \le \varepsilon_{\sigma 2}, \tag{35}$$

where $\varepsilon_{\sigma 1} > 0$ and $\varepsilon_{\sigma 2} > 0$.

Take the following nonlinear robust terms u_{s21} and u_{s22}, which satisfy Eqs. (33), (34) and (35) :

$$u_{s21} = -\frac{h_\sigma^2}{4\varepsilon_{\sigma 1}}\sigma_2 = -k_{21}\sigma_2, \tag{36}$$

$$u_{s22} = -\frac{\left[(1+\rho_2)\hat{\delta}_d\right]^2}{4\varepsilon_{\sigma 2}}\sigma_2 = -k_{22}\sigma_2. \tag{37}$$

The state observation error of the observer designed in the third part is bounded, and $(1+\rho_2) \ge 1$. Therefore, $h_\sigma = h_\sigma(t)$ in Eq. (36) should be chosen to satisfy:

$$h_\sigma(t) \ge (1+\rho_2)\left(\theta_{2\max}|\tilde{x}_2| + \left|\tilde{f}\right|\right). \tag{38}$$

When the nonlinear robust terms u_{s21} and u_{s22} are designed, Eq. (33) is obviously satisfied. Eqs. (34) and (35) are proved to hold as follows.

Substituting Eq. (38) and Eq. (36) into Eq. (34), we could get:

$$\begin{aligned} \sigma_2\left[u_{s21} + (1+\rho_2)\left(\hat{\theta}_2\tilde{x}_2 + \tilde{f}\right)\right] &\le \sigma_2\left\{-\frac{\left[(1+\rho_2)\left(\theta_{2\max}|\tilde{x}_2| + \left|\tilde{f}\right|\right)\right]^2}{4\varepsilon_{\sigma 1}}\sigma_2 + (1+\rho_2)\left(\theta_{2\max}|\tilde{x}_2| + \left|\tilde{f}\right|\right)\right\} \\ &\le -\left[\frac{(1+\rho_2)\left(\theta_{2\max}|\tilde{x}_2| + \left|\tilde{f}\right|\right)\sigma_2}{2\sqrt{\varepsilon_{\sigma 1}}}\right]^2 \\ &\quad + 2\frac{1}{2\sqrt{\varepsilon_{\sigma 1}}}\sqrt{\varepsilon_{\sigma 1}}(1+\rho_2)\left(\theta_{2\max}|\tilde{x}_2| + \left|\tilde{f}\right|\right)\sigma_2 - \varepsilon_{\sigma 1} + \varepsilon_{\sigma 1} \\ &\le -\left[\frac{(1+\rho_2)\left(\theta_{2\max}|\tilde{x}_2| + \left|\tilde{f}\right|\right)\sigma_2}{2\sqrt{\varepsilon_{\sigma 1}}} - \sqrt{\varepsilon_{\sigma 1}}\right]^2 + \varepsilon_{\sigma 1} \\ &\le \varepsilon_{\sigma 1}. \end{aligned} \tag{39}$$

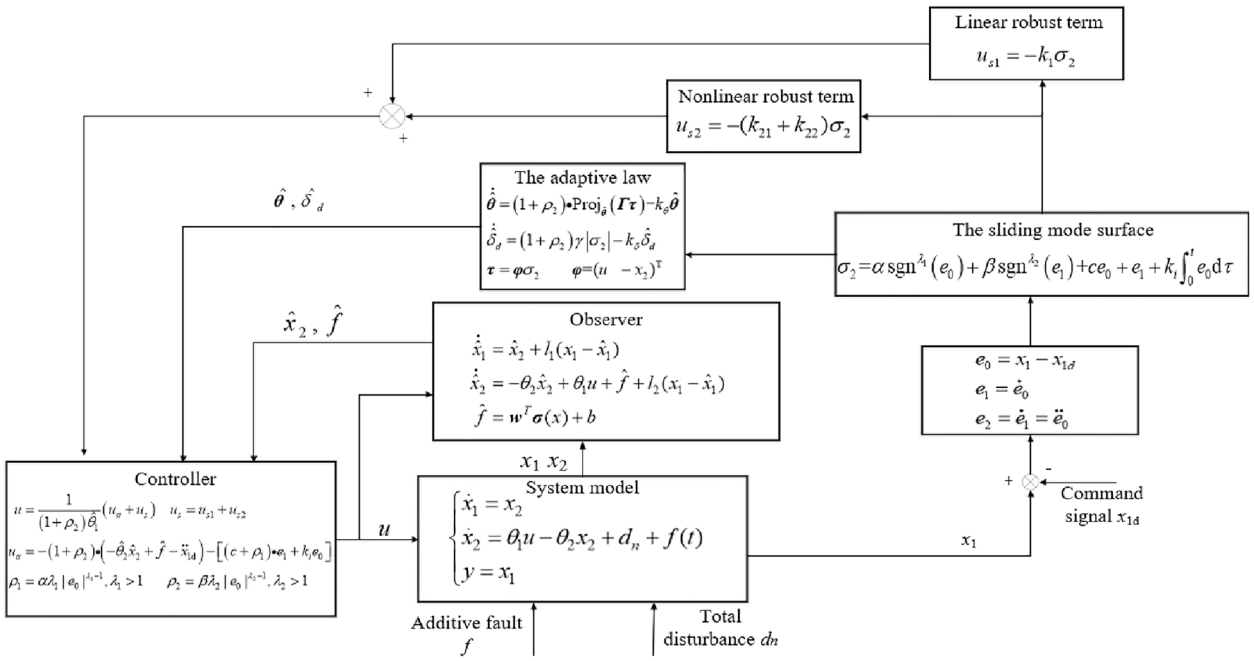

Figure 3 Structure diagram of parameter adaptation and SVM based non-singular terminal sliding mode control strategy

Therefore, Eq. (34) holds.

Substituting Eq. (37) into Eq. (35), we could obtain:

$$\begin{aligned}\sigma_2\left[u_{s22}+(1+\rho_2)\left(d_n+\tilde{\delta}_d\mathrm{sgn}(\sigma_2)\right)\right]&=-\frac{\left[(1+\rho_2)\hat{\delta}_d\right]^2}{4\varepsilon_{\sigma 2}}\sigma_2^2+(1+\rho_2)\left[d_n\sigma_2+\left(\hat{\delta}_d-\delta_d\right)|\sigma_2|\right]\\&\le-\left[\frac{(1+\rho_2)\hat{\delta}_d\sigma_2}{2\sqrt{\varepsilon_{\sigma 2}}}\right]^2+2\frac{1}{2\sqrt{\varepsilon_{\sigma 2}}}\sqrt{\varepsilon_{\sigma 2}}(1+\rho_2)\hat{\delta}_d|\sigma_2|-\varepsilon_{\sigma 2}+\varepsilon_{\sigma 2}\\&\le-\left[\frac{(1+\rho_2)\hat{\delta}_d|\sigma_2|}{2\sqrt{\varepsilon_{\sigma 2}}}-\sqrt{\varepsilon_{\sigma 2}}\right]^2+\varepsilon_{\sigma 2}\\&\le\varepsilon_{\sigma 2}.\end{aligned}\tag{40}$$

Therefore, Eq. (35) holds.

The overall control strategy structure designed in this section is shown in Figure 3.

Lemma 1 (Barbalet lemma) [24] If $x:[0,\infty)\in R$ is uniformly continuous, and when $\lim_{t\to\infty}\int_0^t x(\tau)\mathrm{d}\tau$ exists and is bounded, then $\lim_{t\to\infty}x(t)=0$.

Lemma 2 [25] For the parameter vector θ, $\hat{\theta}$, $\tilde{\theta}$, $\tilde{\theta}=\hat{\theta}-\theta$, the following inequality holds:

$$-tr(\tilde{\theta}^{\mathrm{T}}\hat{\theta})=-\tilde{\theta}^{\mathrm{T}}\hat{\theta}\le-\frac{1}{2}||\tilde{\theta}||_F^2+\frac{1}{2}||\theta||_F^2=-\frac{1}{2}\tilde{\theta}^{\mathrm{T}}\tilde{\theta}+\frac{1}{2}\theta^{\mathrm{T}}\theta,\tag{41}$$

$tr(\cdot)$ represents the trace of the matrix, and $||\cdot||_F$ is the F-norm of the matrix $\cdot$.

Theorem 2 *The controller Eq.* (27) *with observer Eq.* (12), *parameter adaption law Eq.* (29) *and disturbance upper bound adaption law Eq.* (31) *can ensure that the system can achieve asymptotical stability.*

Proof See the Appendix.

Remark 3 Based on the above analysis, for the electromechanical position servo system, the designed controller can achieve asymptotical convergence of tracking error, which is superior to many advanced fault tolerant controllers. The observations based on the SVM can be used to compensate the additive faults in the system.

The state estimation of the observer (12) can be used to reconstruct the controller and under the action of the adaptive law (29) and (31), the system status x_1 can accurately track the desired instruction x_{1d}. What's more, the designed active fault-tolerant controller (27) is continuous and non-singular which is convenient for implementation in engineering application. In addition, the parameter estimation can help diagnose the specific faults since the faults can be reflected by the parameters variation.

Remark 4 There are many parameters in the designed controller and a guideline on how to choose these parameters is given as follows. α is the coefficient before the sign function term of the tracking error, β is the coefficient in front of the sign function term of the tracking error derivative. Increasing α will improve the convergence rate of the tracking error, but if it is too large, oscillation will occur. When the tracking error is small, the convergence effect is not very good, but increasing β can improve the convergence speed. λ_1, λ_2 are the exponent of the sign function term, which are generally bigger than 1. c is the coefficient of the tracking error term in the sliding function, and k_i is the coefficient of the tracking error derivative term. Generally, the larger the value is, the faster the tracking error converges. k_σ is the gain of the robust term, and increasing k_σ will make the system more robust in the presence of external disturbances.

5 Simulation and Analysis

In order to verify the effectiveness of non-singular terminal sliding mode active fault tolerant control, the comparison will be made with the simulation results of four kinds of controllers. The parameters of the four controllers are as follows:

(1) PID: PID controller is the most common close-loop feedback controller in industrial application. It is composed of three parts, including proportional unit P, integral unit I and differential unit D. The corresponding three parameters are set as follows: $k_p = 12$, $k_i = 20$ and $k_d = 0.9$.

(2) TSMC: The terminal sliding mode controller is a nonlinear sliding mode controller which can make the system converge to the equilibrium state in finite time [22]. Its parameters are set as follows: $\alpha = 20$, $\beta = 210$, $\lambda_1 = 10$, $\lambda_2 = 8$, $c = 40$, $k_i = 50$, $k_1 + k_{21} + k_{22} = 65$, $k_\theta = 0.1$, $\gamma = 10$, $k_\delta = 0.1$. The control parameters are choose as $\boldsymbol{\Gamma} = \text{diag}\{150, 50\}$ and the initial estimated value of $\boldsymbol{\theta}$, $\hat{\boldsymbol{\theta}}$ is chosen as [1, 8]. The real value of $\boldsymbol{\theta}$ is [7.8, 0.8].

(3) TSMC-RBF: The RBF based terminal sliding mode fault tolerant controller uses RBF NN to detect the faults and compensate the faults. The specific design is similar to the design procedure in Section 3 and RBF instead of SVM is used here, and the specific parameters are as follows: $b = 100$, $c_1 = 110$, $c_2 = 15$, $q = 29$, $p = 31$, $k_1 + k_{21} + k_{22} = 0.5$, $c = \begin{pmatrix} 1 & 1.3 & 0.61 & 0.91 & 1.5 \\ 1 & 1.3 & 0.61 & 0.91 & 1.5 \end{pmatrix}$, $w_i = 0$.

(4) TSMC-SVM: The SVM based non-singular terminal sliding mode fault tolerant controller proposed in this paper. The specific parameters are as follows: $\alpha = 20$, $\beta = 210$, $\lambda_1 = 10$, $\lambda_2 = 8$, $c = 40$, $k_i = 30$, $k_1 + k_{21} + k_{22} = 60$, $k_\theta = 0.2$, $\gamma = 10$, $k_\delta = 0.1$. The control parameters are chosen as $\boldsymbol{\Gamma} = \text{diag}\{150, 50\}$ and the initial estimated value of $\boldsymbol{\theta}$, $\hat{\boldsymbol{\theta}}$ is chosen as [8, 1]. The real value of $\boldsymbol{\theta}$ are [7.8, 0.8]. The initial estimate of the upper bound of the disturbance $\hat{\delta}_d(0) = 0$.

Table 1 Performance indexes of each controller in simulation in the composite case

Controller	*Me* (°)	μ(°)	σ(°)
PID	0.0077	0.0035	0.0019
TSMC	5.4775×10^{-4}	2.3502×10^{-4}	1.3445×10^{-4}
TSMC-RBF	1.7324×10^{-4}	4.3329×10^{-5}	2.2648×10^{-5}
TSMC-SVM	3.6067×10^{-5}	2.5073×10^{-5}	1.5288×10^{-5}

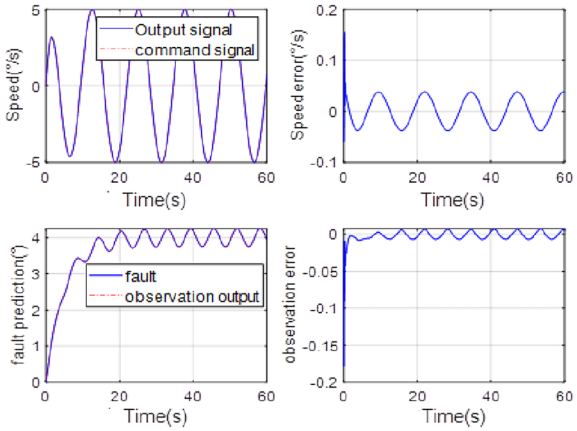

Figure 4 Velocity errors and estimation of additive faults

The desired trajectory is set as $x_{1d} = 10(1 - e^{-0.5t})\sin(0.5t)$. There are additive faults $f = (1 - e^{-t})(4 + 0.01x_1x_2)$ (N·m) and time-varying disturbances $d_n = x_1x_2$(N·m) in the system, and the moment of inertia is reduced to 0.5 times of the original. The simulation results of the three controllers in the above system are as follows.

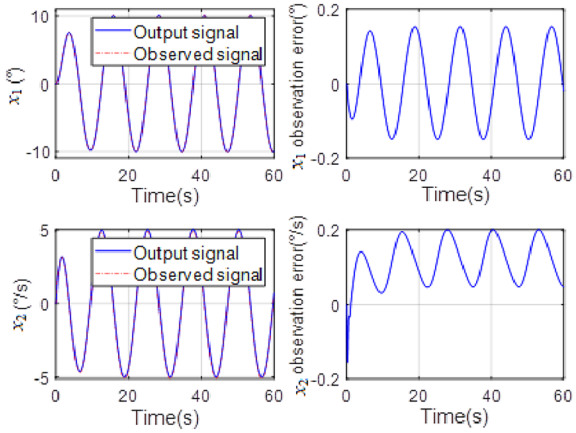

Figure 5 Observation value and observation error of x_1, x_2 of nonlinear observer without fault compensation before the fault-tolerant control is implemented

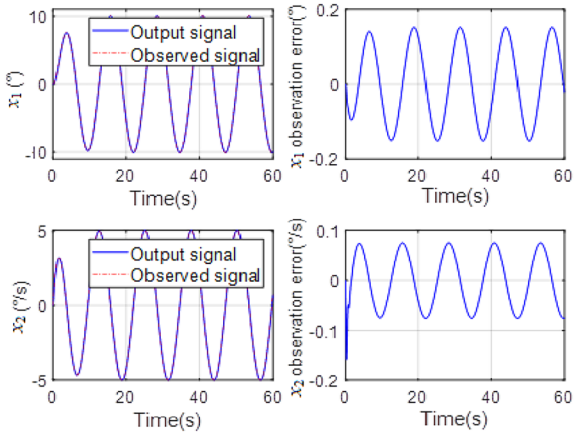

Figure 6 Observation value and observation error of x_1, x_2 of nonlinear observer with fault compensation before the fault-tolerant control is implemented

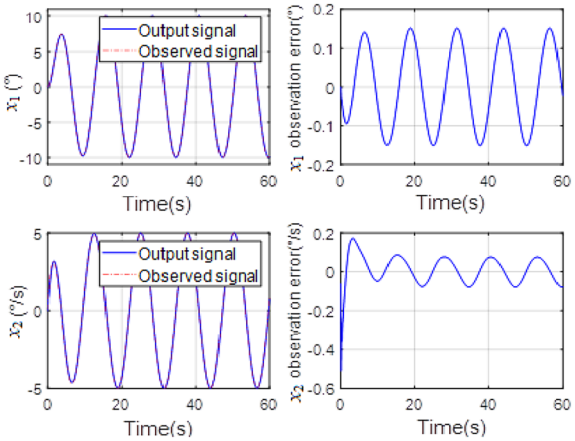

Figure 7 Observation value and observation error of x_1, x_2 of nonlinear observer with fault compensation after the fault-tolerant control is implemented

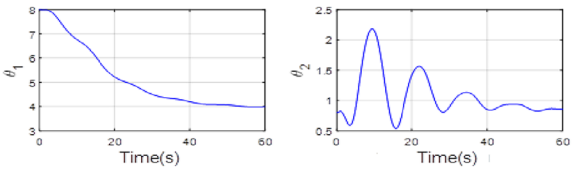

Figure 8 Parameter estimation curves

To evaluate the control performance of each controller, the following evaluation indexes are adopted as in Table 1.

The three performance indexes *Me*, μ, σ, that is to say, the maximum, average, and standard deviation of the tracking errors, are used to evaluate the quality of each control strategy, and their definitions are made as follows:

1) Maximal absolute value of the tracking errors is used as an index of measure of tracking accuracy and is defined as:

$$Me = \max_{i=1,\ldots,M} \{|e(i)|\}, \tag{42}$$

where M is the number of the recorded digital signals.

2) Average tracking error is defined as:

$$\mu = \frac{1}{M}\sum_{i=1}^{M}|e(i)|, \tag{43}$$

and is used as an objective numerical measure of average tracking performance.

3) Standard deviation performance index is defined as:

$$\sigma = \sqrt{\frac{1}{M}\sum_{i=1}^{M}(|e(i)| - \mu)^2}, \tag{44}$$

to measure the deviation level of tracking errors.

As can be seen from Figure 4, the fault estimation error of the fault detection method based on SVM is very small, which helps the controller estimate the fault and compensate it leading to a good robustness to the fault. In addition, the speed tracking error is held within a small range.

Figures 5 and 6 show the estimation performance of the observer without fault compensation and the observer with fault compensation before the fault-tolerant control is implemented. From them, we can see that the estimation error of the observer without fault compensation is obviously larger than that of the observer with fault compensation, especially for the velocity estimation error while the former is 0.2°/s and

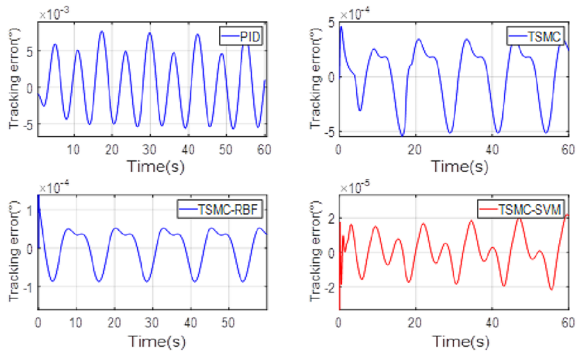

Figure 9 Position tracking error

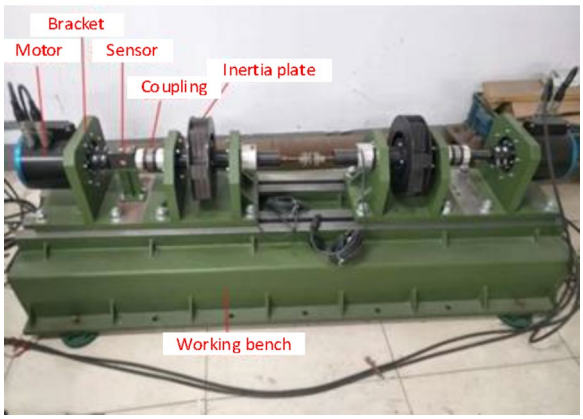

Figure 10 Experimental bench structure

the latter is less than 0.1°/s. This shows that we could use the estimation error of the observer without fault compensation to help us detect the fault and use estimation value of the observer with fault compensation to reconfigure the fault-tolerant controller.

Figure 7 shows the estimation performance of the observer with fault compensation after the fault-tolerant control is implemented. We could see that the observer can estimate the position and speed of the system precisely since the faults have been compensated both in the observer and in the controller. At this time the observed states could help to reconstruct system states in the controller designed in Section 4.

From Figure 8, we could see that the system parameter estimation can converge to a certain range near the real value and thus help the controller to compensate model parameter uncertainty. In addition, it also could help us diagnose the faults since the parameters variation can reflect specific faults.

Finally, it can be seen from Figure 9 and Table 1 that the terminal sliding mode controller has a higher control accuracy and faster response speed than that of PID in the same working condition, while the performance of the non-singular terminal sliding mode active fault-tolerant controller is better than that of terminal sliding mode controller, due to the design of active fault-tolerant control strategy. In addition, compared with TSMC-RBF, TSMC-SVM has higher accuracy and better stability which shows that SVM has a better nonlinearity fitness performance according to a small sample data than RBF.

6 Experiment and Analysis

In order to verify the effectiveness of the algorithm mentioned in this paper, the non-singular terminal sliding mode fault-tolerant control algorithm is experimentally studied and compared with PID and non-singular terminal sliding mode algorithm in terms of control accuracy and response speed. The structure of the experimental platform is shown in Figure 10.

The experimental platform consists of a base, a pair of permanent magnet synchronous motors, electric drivers and rotary encoders with an accuracy of ±13 s, inertia plate, power supply, and a measurement and control system. The left servo channel is used to simulate the high-precision motion control of aero electromechanical system, and the right servo channel is used to simulate faults and disturbances. An industrial computer with a real-time operating system RTU and monitoring software is the kernel part of the measurement and control system. C language is used to write the control program. A 16-bit digital/analog (D/A) conversion card for sending control commands and a 16-bit acquisition card for collecting the position information of the photoelectric encoder are equipped in the computer. The control cycle is 0.5 ms. The system velocity is generated by the backward difference of the high precision position signal. Meanwhile, a second-order Butterworth filter with a cut-off frequency of 50 Hz is used to restrain the measured noise in the speed signal.

Four controllers are tested for the desired trajectory $x_{1d} = 10(1 - e^{-0.5t})\sin(0.5t)°$ and three cases are tested for this motion trajectory. The three cases are as follows:

1) Fault case: Only an additive fault is added in the system and the additive fault $f = (1 - e^{-t})(4 + 0.01x_1x_2)$ (N·m).
2) Time-varying disturbances case: To verify the fault-tolerant control performance of the controller in the presence of external disturbances, a time-varying disturbances $d_n = x_1x_2$ (N·m) with a fault as in case 1 are added to the system.
3) Composite case: In this case, in addition to the time-varying disturbances and a fault as in case 2 added to the system, the moment of inertia of the system

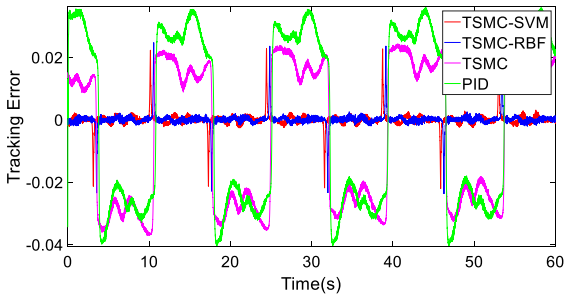

Figure 11 Tracking error in fault case

Table 2 Performance indexes of each controller in fault case

Controller	*Me* (°)	μ (°)	σ (°)
PID	0.0369	0.0324	0.0215
TSMC	0.0271	0.0266	0.0059
TSMC-RBF	0.0247	0.0011	0.0023
TSMC-SVM	0.0230	9.3360×10^{-4}	0.0021

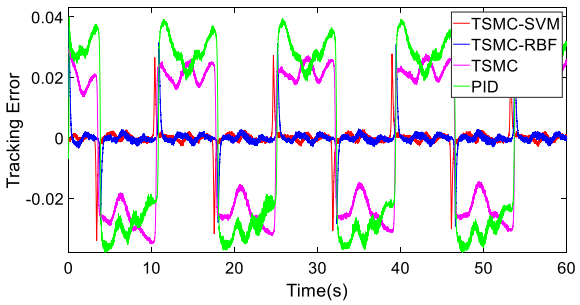

Figure 12 Tracking error in time-varying disturbances

changes, which is reduced to 0.5 times of the original value.

The four controllers are the same as those in the simulation part and their experimental parameters are as follows:

(1) PID: The three parameters are: $k_p = 2500$, $k_i = 210$, $k_d = 100$.
(2) TSMC: The terminal sliding mode parameters are as follows: $\alpha = 20$, $\beta = 210$, $\lambda_1 = 100$, $\lambda_2 = 800$, $c = 100$, $k_i = 50$, $k_1 + k_{21} + k_{22} = 120$. The other parameters are the same as the simulation.
(3) TSMC-RBF: The parameters are: $w_i = 0$, $b = 100$, $c = \begin{pmatrix} 1 & 1.3 & 0.61 & 0.91 & 1.5 \\ 1 & 1.3 & 0.61 & 0.91 & 1.5 \end{pmatrix}$, $\alpha = 20$, $\beta = 210$, $\lambda_1 = 100$, $\lambda_2 = 800$, $c = 100$, $k_i = 3$, $k_1 + k_{21} + k_{22} = 120$.

Table 3 Performance indexes of each controller in the time-varying disturbances case

Controller	*Me* (°)	μ (°)	σ (°)
PID	0.0391	0.0424	0.0227
TSMC	0.0431	0.0232	0.0046
TSMC-RBF	0.0367	0.0017	0.0045
TSMC-SVM	0.0338	0.0016	0.0041

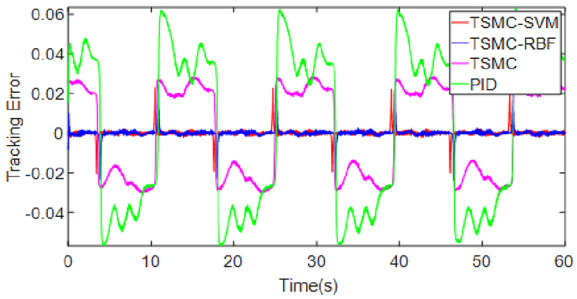

Figure 13 Tracking error in parameter perturbation

Table 4 Performance indexes of each controller in the composite case

Controller	*Me* (°)	μ (°)	σ (°)
PID	0.0618	0.0483	0.0256
TSMC	0.0365	0.0229	0.0044
TSMC-RBF	0.0238	0.0037	0.0031
TSMC-SVM	0.0208	0.0036	0.0025

(4) TSMC-SVM: The parameters are: $\alpha = 20$, $\beta = 210$, $\lambda_1 = 100$, $\lambda_2 = 800$, $c = 100$, $k_i = 3$, $k_1 + k_{21} + k_{22} = 120$. The other parameters are the same as those in the simulation.

To test the effectiveness of the proposed fault-tolerant control algorithm, an additive fault is added in the system in case 1. The tracking performance of the four controllers in fault case is shown in Figure 11 and Table 2. As can be seen, the performance of TSMC is better than that of PID since PID has no adaptive ability and cannot identify the fault and compensate it while TSMC has certain robustness to faults. By employing the proposed fault detection observer to estimate the fault and compensate them, both TSMC-RBF and TSMC-SVM controllers have better performance than the other two controllers. However, TSMC-SVM has higher control accuracy and response speed than those of TSMC-RBF since SVM is superior to RBF in solving small sample approximation problem.

To further test the effectiveness of the proposed fault-tolerant control algorithm in the presence of external disturbances and the fault, case 2 has been carried out. As can be seen from Figure 12 and Table 3, the control accuracy of TSMC-SVM decreased compared to that in case 1, since external disturbances has increased the influence of the system model uncertainties on control accuracy. However, the TSMC-SVM controller still has the highest control accuracy and the fastest response speed among the four controllers. That is because the fault can be identified by SVM accurately and compensated in the controller and the influence of disturbances and compensation error can be overcome by the non-singular terminal sliding mode control law. In addition, SVM is superior to RBF in solving small sample approximation problem. Thus in case 2 the TSMC-SVM controller shows better performance than the other controllers.

In order to test the effectiveness of the proposed fault-tolerant control algorithm in the most complex and poor working condition, in which there exist disturbances, parameter perturbation and the faults simultaneously, case 3 has been implemented. As seen from Figure 13 and Table 4, the control accuracy of TSMC-SVM further decreased compared to that in case 1 and case 2, since both external disturbances and parameter perturbation have further increased the influence of the system model uncertainties on control accuracy. However, the TSMC-SVM controller still has the highest control accuracy and the fastest response speed among the four controllers, since the fault can be identified by SVM accurately and compensated, the parameter perturbation can be captured by the adaptive law of TSMC-SVM which helps reduce the total uncertainties greatly, and the influence of disturbances can be overcome by the non-singular terminal sliding mode control law. In addition, since SVM is better than RBF in solving small sample approximation problem, the TSMC-SVM controller shows better performance than the other controllers in case 3.

7 Conclusions

In this paper, a fault tolerant non-singular terminal sliding mode control method based on support vector machine (SVM) is proposed for aeronautics electromechanical system subjected to system fault, the parametric uncertainty and unknown bounded disturbances. SVM is designed to estimate the possible faults in the system by off-line learning from a small sample data, which helps estimate the fault and compensate it in the proposed controller. An observer is designed to estimate the system states to make fault detection and reconstruct the states in the controller when something malfunctions in electromechanical system. A fault tolerant non-singular terminal sliding mode controller with the SVM based observer is designed, and Lyapunov theorem is used to prove its asymptotical stability. Extensive comparative simulation and experimental results illustrate the effectiveness and advancement of the proposed controller compared with several other main-stream controllers.

Appendix

Proof of theorem 1

For the dynamic equation of system observation error Eq. (13), the Lyapunov function is chosen as follows:

$$V(\boldsymbol{e}_x) = \frac{1}{2}\boldsymbol{e}_x^{\mathrm{T}}\boldsymbol{P}\boldsymbol{e}_x. \tag{45}$$

The time-based differential of Eq. (45) is:

$$\begin{aligned}
\dot{V}(\boldsymbol{e}_x) =& \frac{1}{2}\dot{\boldsymbol{e}}_x^{\mathrm{T}}\boldsymbol{P}\boldsymbol{e}_x + \frac{1}{2}\boldsymbol{e}_x^{\mathrm{T}}\boldsymbol{P}\dot{\boldsymbol{e}}_x \\
=& \frac{1}{2}\left[(\boldsymbol{A}-\boldsymbol{L}\boldsymbol{C})\boldsymbol{e}_x + \boldsymbol{D}\left(d_n + f - \hat{f}\right)\right]^{\mathrm{T}}\boldsymbol{P}\boldsymbol{e}_x \\
=& \frac{1}{2}\boldsymbol{e}_x^{\mathrm{T}}\left(\boldsymbol{A}_o^{\mathrm{T}}\boldsymbol{P} + \boldsymbol{P}\boldsymbol{A}_o\right)\boldsymbol{e}_x + \boldsymbol{e}_x^{\mathrm{T}}\boldsymbol{P}\boldsymbol{D}\left(d_n + f - \hat{f}\right) \\
\le& -\frac{1}{2}\lambda_{\min}(\boldsymbol{Q})\|\boldsymbol{e}_x\|^2 + \left|\boldsymbol{e}_x^{\mathrm{T}}\boldsymbol{P}\boldsymbol{D}\right|(F+\delta_d) \\
\le& -\frac{1}{2}\lambda_{\min}(\boldsymbol{Q})\|\boldsymbol{e}_x\|^2 + \frac{1}{2}\|\boldsymbol{e}_x\|^2 + \frac{1}{2}[\lambda_{\max}(\boldsymbol{P})(F+\delta_d)]^2 \\
\le& -\frac{1}{2}[\lambda_{\min}(\boldsymbol{Q})-1]\|\boldsymbol{e}_x\|^2 + \frac{1}{2}[\lambda_{\max}(\boldsymbol{P})(F+\delta_d)]^2 \\
\le& -\frac{\lambda_{\min}(\boldsymbol{Q})-1}{\lambda_{\max}(\mathbf{P})}\frac{1}{2}\boldsymbol{e}_x^{\mathrm{T}}\boldsymbol{P}\boldsymbol{e}_x + \frac{1}{2}[\lambda_{\max}(\boldsymbol{P})(F+\delta_d)]^2 \\
\le& -\frac{\lambda_{\min}(\boldsymbol{Q})-1}{\lambda_{\max}(\boldsymbol{P})}V + \frac{1}{2}[\lambda_{\max}(\boldsymbol{P})(F+\delta_d)]^2.
\end{aligned} \tag{46}$$

In Eq. (46), $\lambda_{\min}(\boldsymbol{Q})$ represents the minimum eigenvalue of the matrix $\boldsymbol{Q}$, and $\lambda_{\max}(\boldsymbol{P})$ represents the maximum eigenvalue of the matrix $\boldsymbol{P}$. The above inequality can be expressed as follows:

$$\dot{V} \le -\lambda_1 V + \lambda_2. \tag{47}$$

Multiply both sides of the inequality of Eq. (47) by $e^{\lambda_1 t}$ to get:

$$\frac{\mathrm{d}}{\mathrm{d}t}(V(t)e^{\lambda_1 t}) \le e^{\lambda_1 t}\lambda_2. \tag{48}$$

Integrate over [0, t], and the above formula can be obtained:

$$V \le (V(0) - \frac{\lambda_2}{\lambda_1})e^{-\lambda_1 t} + \frac{\lambda_2}{\lambda_1} \le V(0) + \frac{\lambda_2}{\lambda_1}. \tag{49}$$

It is proved that the designed observer is bounded stability.

Proof of theorem 2

Take the Lyapunov function as follows:

$$V(t) = \frac{1}{2}\sigma_2^2 + \frac{1}{2}\boldsymbol{\Gamma}^{-1}\tilde{\boldsymbol{\theta}}^{\mathrm{T}}\tilde{\boldsymbol{\theta}} + \frac{1}{2}\gamma^{-1}\tilde{\delta}_d^2. \tag{50}$$

Its time differential is:

$$\begin{aligned}\dot{V}(t) &= \sigma_2\dot{\sigma}_2 + \boldsymbol{\Gamma}^{-1}\tilde{\boldsymbol{\theta}}^{\mathrm{T}}\dot{\hat{\boldsymbol{\theta}}} + \gamma^{-1}\tilde{\delta}_d\dot{\hat{\delta}}_d \\ &= \sigma_2\left\{-k_1\sigma_3 + u_{s2} + (1+\rho_2)\left(-\tilde{\boldsymbol{\theta}}^{\mathrm{T}}\boldsymbol{\varphi} + \hat{\theta}_2\tilde{x}_2 + d_n + \tilde{f}\right)\right\} \\ &\quad + \boldsymbol{\Gamma}^{-1}\tilde{\boldsymbol{\theta}}^{\mathrm{T}}\dot{\hat{\boldsymbol{\theta}}} + \gamma^{-1}\tilde{\delta}_d\dot{\hat{\delta}}_d.\end{aligned} \tag{51}$$

Since the system state observation error is bounded and the fault estimation error is known to be bounded according to Eq. (11), the adaptive rate Eq. (29) and Eq. (31) are substituted into Eq. (50) to obtain:

$$\begin{aligned}\dot{V}(t) =& -k_1\sigma_3^2 + u_{s2}\sigma_2 + (1+\rho_2)\left(\hat{\theta}_2\tilde{x}_2 + \tilde{f}\right)\sigma_2 \\ &- (1+\rho_2)\tilde{\boldsymbol{\theta}}^{\mathrm{T}}\boldsymbol{\varphi}\sigma_2 + (1+\rho_2)d_n\sigma_2 \\ &+ \boldsymbol{\Gamma}^{-1}\tilde{\boldsymbol{\theta}}^{\mathrm{T}}\left[(1+\rho_2)\cdot\mathrm{Proj}_{\hat{\theta}}(\boldsymbol{\Gamma}\boldsymbol{\tau}) - k_\theta\hat{\theta}\right] \\ &+ \gamma^{-1}\tilde{\delta}_d\left[(1+\rho_2)\gamma|\sigma_2| - k_\delta\hat{\delta}_d\right] \\ =& -k_1\sigma_2^2 + u_{s21}\sigma_2 + (1+\rho_2)\left(\hat{\theta}_2\tilde{x}_2 + \tilde{f}\right)\sigma_2 \\ &+ u_{s22}\sigma_2 + (1+\rho_2)\left(d_n\sigma_2 + \tilde{\delta}_d|\sigma_2|\right) \\ &- (1+\rho_2)\tilde{\boldsymbol{\theta}}^{\mathrm{T}}\boldsymbol{\varphi}\sigma_2 + \boldsymbol{\Gamma}^{-1}\tilde{\boldsymbol{\theta}}^{\mathrm{T}}(1+\rho_2)\cdot\mathrm{Proj}_{\hat{\theta}}(\boldsymbol{\Gamma}\boldsymbol{\tau}) \\ &- k_\theta\boldsymbol{\Gamma}^{-1}\tilde{\boldsymbol{\theta}}^{\mathrm{T}}\hat{\boldsymbol{\theta}} - k_\delta\gamma^{-1}\tilde{\delta}_d\hat{\delta}_d.\end{aligned} \tag{52}$$

Substituting the conditions Eq. (34) and Eq. (35) satisfied by the nonlinear robust term u_{s2} into Eq. (52), the following equation can be obtained:

$$\dot{V}(t) \le -k_1\sigma_2^2 - k_\theta\boldsymbol{\Gamma}^{-1}\tilde{\boldsymbol{\theta}}^{\mathrm{T}}\hat{\boldsymbol{\theta}} - k_\delta\gamma^{-1}\tilde{\delta}_d\hat{\delta}_d + \varepsilon_{\sigma 1} + \varepsilon_{\sigma 2}. \tag{53}$$

Lemma 2 is applied to obtain:

$$\begin{aligned}\dot{V}(t) \le& -k_1\sigma_2^2 - k_\theta\boldsymbol{\Gamma}^{-1}\tilde{\boldsymbol{\theta}}^{\mathrm{T}}\hat{\boldsymbol{\theta}} - k_\delta\gamma^{-1}\tilde{\delta}_d\hat{\delta}_d + \varepsilon_{\sigma 1} + \varepsilon_{\sigma 2} \\ \le& -k_1\sigma_2^2 + k_\theta\boldsymbol{\Gamma}^{-1}\left(-\frac{1}{2}\tilde{\boldsymbol{\theta}}^{\mathrm{T}}\tilde{\boldsymbol{\theta}} + \frac{1}{2}\theta^{\mathrm{T}}\theta\right) \\ &+ k_\delta\gamma^{-1}\left(-\frac{1}{2}\tilde{\delta}_d^2 + \frac{1}{2}\delta_d^2\right) + \varepsilon_{\sigma 1} + \varepsilon_{\sigma 2} \\ \le& -k_1\sigma_2^2 - \frac{1}{2}k_\theta\boldsymbol{\Gamma}^{-1}\tilde{\boldsymbol{\theta}}^{\mathrm{T}}\tilde{\boldsymbol{\theta}} - \frac{1}{2}k_\delta\gamma^{-1}\tilde{\delta}_d^2 \\ &+ \frac{1}{2}k_\theta\boldsymbol{\Gamma}^{-1}\boldsymbol{\theta}^{\mathrm{T}}\boldsymbol{\theta} + \frac{1}{2}k_\delta\gamma^{-1}\delta_d^2 + \varepsilon_\sigma.\end{aligned} \tag{54}$$

In Eq. (54), $\varepsilon_\sigma = \varepsilon_{\sigma 1} + \varepsilon_{\sigma 2} > 0$. Define $\lambda_{\mathrm{k1}} = \min\{2k_1, k_\theta, k_\delta\}$, $\lambda_{\mathrm{k2}} = \frac{k_\theta}{2}\boldsymbol{\Gamma}^{-1}\boldsymbol{\theta}^{\mathrm{T}}\boldsymbol{\theta} + \frac{k_\delta}{2}\gamma^{-1}\delta_d^2 + \varepsilon_\sigma$, Then Eq. (54) can be expressed as:

$$\dot{V} \le -\lambda_{k1}V + \lambda_{k2}. \tag{55}$$

To solve the above differential equation, we can get:

$$V \le \left(V(0) - \frac{\lambda_{k2}}{\lambda_{k1}}\right)e^{-\lambda_{k1}t} + \frac{\lambda_{k2}}{\lambda_{k1}}. \tag{56}$$

Therefore, $\lim_{t\to\infty} V(t) \le \frac{\lambda_{k2}}{\lambda_{k1}}$, the system is bounded and stable. when t goes to infinity, V is bounded, thus σ_2 is bounded, and there are integral terms $\int_0^t e_0 \mathrm{d}\tau$ and bounds in σ_2. According to Lemma 1, $e_0 \to 0$ when $t \to \infty$, and then $x_1 \to x_{1\mathrm{d}}$. Theorem 2 is proved.

Acknowledgements
Not applicable.

Authors' Contributions
JH was in charge of the whole design of the proposed controller and experiment plan, and wrote the manuscript; ZY assisted with sampling data and laboratory analyses; JY modified and improved the wording. All authors read and approved the final manuscript.

Funding
Supported by National Natural Science Foundation of China (Grant No. 51975294) and Fundamental Research Funds for the Central Universities of China (Grant No. 30922010706).

Data Availability
Data is available according to reasonable request.

Declarations

Competing Interests
The authors declare no competing financial interests.

Received: 2 June 2021 Revised: 2 April 2024 Accepted: 11 April 2024
Published online: 03 June 2024

References

[1] N J Groom. *Electric flight system*. NASA Conference Publication, 1982.
[2] J E Jackson, E Espenschied, J Klop. The control system for the X-33 linear aerospike engine. *IEEE Aerospace Applications Conference Proceedings*, 1998, 3: 181-191.
[3] L Fan, H Huang, K Zhou. Robust fault tolerant attitude control for satellite with multiple uncertainties and actuator faults. *Chinese Journal of Aeronautics*, 2020, 33(12): 3380-3394.
[4] T Li, Z Jiang, S Zhang. Reconfigurable fault tolerant control for supersonic missiles with actuator failures under actuation redundancy. *Chinese Journal of Aeronautics*, 2020, 33(1): 324-338.
[5] M Liu, D Ho, P Shi. Adaptive fault-tolerant compensation control for Markovian jump systems with mismatched external disturbance. *Automatica*, 2015, 58(1): 5-14.

[6] K S Lee, T G Park. An actuator fault reconstruction scheme for linear systems. *Journal of Process Control*, 2016, 44: 106-119.
[7] Dekys, Vladimir. Condition monitoring and fault diagnosis. *Procedia Engineering*, 2017, 177: 502-509.
[8] H Yang, H Luo, O KAYNAK. Adaptive SMO-based fault estimation for Markov jump systems with simultaneous additive and multiplicative actuator faults. *IEEE Systems Journal*, 2020, 15(7): 607-616.
[9] P Garimella, B Yao, Nonlinear adaptive robust observer design for a class of nonlinear systems. *Proceedings of the American Control Conference*, 2003, (5): 4391-4396.
[10] P Garimella, B Yao. Robust model-based fault detection using adaptive robust observers. *Proceedings of the 44th IEEE Conference on Decision and Control*, 2005: 3073-3078.
[11] P Garimella, B Yao. Model based fault detection of an electro-hydraulic cylinder. *Proceedings of the American Control Conference*, 2005: 484-489.
[12] S Gayaka, B Yao. Fault detection, identification and accommodation for an electro-hydraulic system: An adaptive robust approach. *17th IFAC World Congress*, 2008: 13815-13820.
[13] Q Shen, B Jiang, P Shi, et al. Novel neural networks-based fault tolerant control scheme with fault alarm. *IEEE Trans. Cybern.*, 2014, 44(11): 2190–2201.
[14] M Chen, R Mei. Actuator fault tolerant control for a class of nonlinear systems using neural networks. *11th IEEE International Conference on Control & Automation (ICCA)*, 2014: 101–106.
[15] S Zhang, P Yang, L Kong, et al. Neural networks-based fault tolerant control of a robot via fast terminal sliding mode. *IEEE Trans. Ind. Electron*, 2021, 51(7): 4091-4101.
[16] Y Yao, X Zhang. Fault diagnosis approach for roller bearing based on EMD momentary energy entropy and SVM. *Journal of Electronic Measurement and Instrumentation*, 2013, 27(10): 957-962.
[17] Y Xu, X Zhao, W Yang, et al. Planetary gear fault diagnosis based on information fusion of multi parameters and multi points. *Chinese Journal of Scientific Instrument*, 2014, 35(8): 1789–1795.
[18] B Yan, X J Wang, Z G Jiang. Study on the gaze estimation algorithm based on support vector regression model. *Chinese Journal of Scientific Instrument*, 2014, 35(10) : 2299-2305.
[19] R Salat, S Osowski. Accurate fault location in the power transmission line using support vector machine approach. *IEEE Transactions on Power Systems*, 2004, 19(2): 979-986.
[20] R Fu, B Li, Y Gao, et al. Content-based image retrieval based on CNN and SVM. *2016 2nd IEEE International Conference on Computer and Communications (ICCC)*, 2016: 638-642.
[21] J Mathew, M Luo, C K Pang. Regression kernel for prognostics with support vector machines. *2017 22nd IEEE International Conference on Emerging Technologies and Factory Automation (ETFA)*, 2017: 1-5.
[22] A Awad, H Wang. Roll-pitch-yaw autopilot design for nonlinear time-varying missile using partial state observer based global fast terminal sliding mode control. *Chinese Journal of Aeronautics*, 2016, 29(5): 1302–1312.
[23] Q Jia, B N Yuan, G Chen, et al. Adaptive fuzzy terminal sliding mode control for the free-floating space manipulator with free-swinging joint failure. *Chinese Journal of Aeronautics*, 2021, 34(9): 178-198.
[24] G Tao. A simple alternative to the Barbalat lemma. *IEEE Transactions on Automatic Control*, 1997, 42(5): 698.
[25] C Xu, J Hu. Adaptive robust control of a class of motor servo system with dead zone based on neural network and extended state observer. *Proceedings of the Institution of Mechanical Engineers, Part I: Journal of Systems and Control Engineering*, 2022, 236(9): 1724–1737.

Jian Hu born in 1980, received her B.S. degree in measurement and control technology and instruments from *Southeast University, China,* in 2002. She received the PhD degree in precise instruments and machinery from *Southeast University, China,* in 2007. From 2007 to 2017, she was an assistant professor in *Nanjing University of Science and Technology*. In 2013, she was a visiting scholar at *Henry Samueli School of Engineering, UC Irvine, Irvine, USA*. Since 2017, she has been an associate professor at *School of Mechanical Engineering, Nanjing University of Science and Technology, China*. Her current research interests include servo control of mechatronic systems, intelligent control, and artificial intelligence technology and application.

Zhengyin Yang born in 1998, obtained a Master's degree in mechanical and electronic engineering from *Nanjing University of Science and Technology, China,* in 2023. His main research direction is servo control of mechatronic integrated systems and intelligent algorithms.

Jianyong Yao born in 1984, received his B.Tech. degree from *Tianjin University, China*, in 2006, and the PhD degree from *Beihang University, China*, in 2012, both in mechatronics. He was a visiting exchange student at *School of Mechanical Engineering, Purdue University*, *U.S.A.,* from October 2010 to October 2011. In 2012, he joined *School of Mechanical Engineering, Nanjing University of Science and Technology, China*, where he is currently a full professor. His current research interests include servo control of mechatronic systems, adaptive and robust control, fault detection, and accommodation of dynamic systems.